T. Yehoshua, A Seifert
(School of Mechanical Engineering,
Faculty of Engineering
TelAvivUniversity)

E-mail: seifert@eng.tau.ac.il

Empirical Model for the Evolution of a Vortex-Pair Introduced into a Boundary Layer

A linear, empirical, low-order-model was developed with the aim of describing the evolution of a 2D vortex-pair ejected into a boundary layer from a slot-in-the-wall. The model describes the evolution of a counter-rotating pair of Lamb-Oseen vortices in the proximity of a wall on which a cross-flow Blasius boundary layer exits. Two inputs from experimental measurements are used. First, the initial locations where the vortices form and pinch-off from the excitation slot boundary layers. Second, the time evolution of the vortex circulation in still-air. With this input, the model predicts the trajectories and vorticity distribution during the interaction. Such a model could be a viable tool for the development of a low-order-model to be implemented as a simplified boundary condition in CFD simulations, with the aim of reducing the requirement to fully resolve the vicinity of the excitation slot in active flow control simulations.

Introduction

In the words of Saffman [1] relating to vortex rings: "…one particular motion exemplifies the whole range of problems of vortex motion… vortex rings…Their formation is a problem of vortex sheet dynamics, the steady-state is a problem of existence, their duration is a problem of stability and if there are several, we have a problem of vortex interactions". It could be added, if we generate desired vortices in a shear layer – we have flow control. Boundary layer sensitivity and adaptivity to high-amplitude periodic-excitation emanating from a slot-in-the-wall is a determining stage in the efficacy of Active Flow Control (AFC) systems. Understanding the governing mechanisms of this interaction and identifying its leading parameters and their optimal values, will allow the boundary layer evolution (e.g., separation delay) to be managed efficiently. Arriving at a CFD design tool is of immense practical importance while the necessity of properly resolving the actuator-slot region is a limiting factor. Therefore, modeling the interaction and providing a low-order, simplified boundary condition for CFD simulation is highly desired.

The inherent complication of even the most conventional AFC application, such as boundary layer reattachment, is expressed by the large parameter space that the designer must optimize. This parameter space is a collection of the baseline flow parameters (boundary layer Reynolds number, turbulent vs. laminar flow, pressure gradient, curvature and more) as well as the excitation parameters (steady vs. oscillatory, slot/hole location and orientation, magnitude (peak slot exit velocity is currently used), frequency and more, as presented by the relevant Strouhal, Reynolds and Stokes numbers.

The aim of the experimental part of the study [2-4] was to methodically isolate and document the effects of the governing parameters of this complicated problem, with an emphasis on the excitation parameters. The huge parameter space was limited to the case of a laminar boundary-layer with zero pressure-gradient and to Zero-Mass-Flux (ZMF) oscillatory excitation from a slot-in-the-wall. The key parameters under study were the excitation magnitude, frequency, orientation (wall normal, upstream or downstream directed shallow-angle excitation) and frequency (only pure sine excitation would be considered here), maintaining nominally 2D conditions. Two-dimensional Particle Image Velocimetry (PIV) measurements, as well as hot-wire, temperature and pressure measurements were performed, in order to achieve high spatial and temporal resolution of the physical processes taking place during the complex interaction.

The nature of the excitation in quiescent fluid was initially studied [2], [4], in order to document the effect of each of the leading parameters without the presence of the cross-flow boundary layer. The measurements show that different boundary conditions at the actuator's exit-slot dictate an entirely different vorticity dynamics, which results in different initial vortex circulation, different formation locations, different decay rates and circulation signs that "survive" to later interact with the boundary layer and significantly different vortex convection velocities.

A threshold excitation magnitude was identified, in agreement with published vortex escape criteria [5]. When the excitation magnitude was lower than the threshold, the vortices were sucked back into the actuator cavity and the average external flow field remained practical-

ly stagnant. For supercritical cases, in which the excitation magnitude was sufficient to release vortices, the vortex circulation and convection velocity were found to approximately scale with the excitation magnitude [4].

The interaction of the excitation with the cross-flow laminar-boundary-layer was measured and is currently being analyzed and modeled. The excitation direction was found to be a leading parameter when considering the resulting vorticity dynamics. Details of the vortex circulation and trajectories will be presented and compared to the model. In practical terms, upstream directed excitation was the most effective in tripping a sub-critical boundary layer [3]. Downstream directed excitation was proven to be the most efficient for applications such as boundary layer reattachment due to the increased skin-friction, whereas wall-normal excitation was the least effective configuration tested in the context of practical active flow control applications. However, for simplicity and convenience, we initially model the wall-normal excitation boundary-layer interaction.

The process of vortex generation due to high-amplitude slot or hole excitation is tightly linked to the physical process enabling the generation of vortex rings in still fluid [6]. The vorticity ejected from the inner slot-channel during the blowing part of the cycle is generally accepted [7] to determine the resulting vortex circulation.

While the analogy to vortex ring generation by a piston-and-cylinder arrangement is quite appealing, especially for ramp-up-ramp-down piston motion, it breaks down because the piston only moves out and comes to a halt. This contrasts with the nature of the ZMF actuator generating high-amplitude excitation, for which half of its operation cycle is characterized by suction.

Models for the development of ZMF excitation in still air are rare. One example can be found in [8], which presents a low-order-model of computationally generated ZMF excitation in still-air. The authors use Proper Orthogonal Decomposition (POD [9]) to model the flow field in the actuator vicinity and show that only four modes are needed to represent this simple flow quite successfully. However, it is clear that this simplicity and low order cannot be maintained in more complex situations and certainly will not be capable of predicting situations dominated by cross-flow, three-dimensionality and transition to turbulence. An idea on the complexity of real-life 3D interaction of jets in cross-flow can be gained from [17].

Models describing vortices moving towards a wall are relevant to the current application, with the motion direction reversed. Such models take into account the image vortex system due to the vicinity of the wall. Lamb [10] proposed a simple model to describe a vortex-pair interaction with a wall. Clearly, away from the wall, the 2D vortices induce a constant velocity on each other, leading to their constant convection rate and straight, wall-normal trajectory. As the vortex pair approaches the wall, the image vortices have a growing effect, pushing the vortices away from each other. The trajectories were also computed as (for constant circulation): $x_1^2\left(x^2+y^2\right)=x^2y^2$, where y is the wall normal direction and x the wall tangential direction, with the origin at the slot exit (see figure 3) and $2x_j$ is the separation between the vortices in the pair far from the wall. Certainly, a family of such trajectories can be found to pass through every set of initial vortex-pair locations, $x=\pm x_j$ and $y=y_j$. The challenge, as in the model to be detailed in this paper, is to select a relevant initial vortex-pair location, and define its circulation based on a given actuator design. More importantly, derive actuator design laws that will maximize the desired alternation in the boundary layer vorticity distribution.

A family of point-vortex models has been developed by Karwiet [11] and Sheffield [12], describing the motion of a vortex pair close to an opening in a wall or a pipe inlet. Case I in the work by Sheffield is actually the closest in geometry to the present wall-normal excitation. As Karweit explains: "if the hole (opening) is large enough, the vortices will pass through; if it is too narrow (relative to the distance between the vortices), they will separate and follow diverging paths without going through". In the words of Sheffield: "If the vortex pair starts too close to the wall, then it will not travel away from the wall, but into the channel". It has been noted experimentally that as the peak velocity of the piston or slot exit velocity increases, not only the vortex circulation increases, but the location from the slot exit in which the vortex reaches its peak circulation and pinches-off also increases. Therefore, knowing the initial vortex location and accepting that its initial location depends on the excitation magnitude will allow the "vortex formation criteria" of Holman et al. [5], which have also been identified in several earlier studies, to be modeled. The Karweit [11] and Sheffield [12] potential flow vortex models use a single vortex placed close to half the width of the opening geometry (assuming a symmetry line) and using the Schwartz-Christoffel transformation to map the flow. In the transformed flow, the Routh [13] quasi-stream-function allows the vortex trajectory to be calculated. Despite its capability to describe the complex behavior of the vortex-pair in the vicinity of the slot, this approach cannot be extended to consider the interaction of the vortex-pair with a cross-flow boundary layer, or even consider the case where the magnitudes or initial locations, or the vortices in the pair, are not identical, as is the case for an inclined slot. Therefore, the development of a numerical model composed of similar elements is warranted. The basic ingredient in every such model is the isolated vortex.

The selection of an isolated vortex model is not straightforward. Many inviscid vortex models exist [14]. It is obvious that for the current application, a point vortex is not suitable. Also, the decay of the vortex circulation during the second half of every excitation cycle cannot be neglected. This effect would be modeled based on experimental findings of a vortex pair evolution in still-air [2-4].

The interaction of the vortex-pair with the external cross-flow boundary-layer will be performed by a simple superimposition of the vortex system with a Blasius boundary layer. Since we are dealing also with the imaged vortex-pair system, the image boundary layer will also be modeled, otherwise the wall could not remain a symmetry line.

The paper includes an empirical mathematical modeling of the excitation developed in still-air and in the presence of a laminar cross-flow boundary-layer. It also provides a detailed comparison with experiments. The experimental set-up will not be presented here. The reader is referred to earlier papers by the current authors for that matter.

Model and Results

Isolated vortex model

The first choice to be made before attempting to model the interaction between high-amplitude excitation with still or co-flowing fluid is the type of vortex model to use. Many models with increasing levels of

complexity exist (e.g., [14],[15]) and it is beyond the scope of this paper to review these options. Rather, an appropriate vortex model can be selected by considering the current experimental results [4].

The choice of a vortex model and its validation should be performed as close as possible to the excitation slot, but after the vortex-pair had been formed. This is because once a vortex model had been selected, only its initial position and circulation will determine the entire evolution sequence and enable its dynamic evolution through the first oscillation cycle to be modeled.

The data presented below clearly shows that the vortices generated by the apparatus described in [4] can be represented fairly well by the two-dimensional Lamb-Oseen vortex model (Lamb [10]; Batchelor [16]) as detailed below and compared to experimental data. The Lamb-Oseen vortex is a solution of the Navier-Stokes-equations only under the assumption of axial symmetry. Axial symmetry can be assumed locally valid only if the distance between the vortices is large compared to their radius. Since the axial symmetry should be allowed to break, to empirically model the experiments, each vortex forming the 2D pair is modeled individually. In the current model we allow the distances between the vortex cores to become of the same order as the vortex radii, and our only justification is success in modeling the interaction.

The circumferential velocity, v_θ, out-of-plane component of vorticity, ω, circulation, Γ and radius scaling factor, δ, of the Lamb-Oseen vortex model are given by the following expressions:

$$v_\theta = \frac{\Gamma_0}{2\pi r}\left[1-\exp\left(-\frac{r^2}{\delta^2}\right)\right] \quad (1)$$

$$\omega = \frac{\Gamma_0}{\pi\delta^2}\exp\left(-\frac{r^2}{\delta^2}\right) \quad (2)$$

$$\Gamma = \Gamma_0\left[1-\exp\left(-\frac{r^2}{\delta^2}\right)\right] \quad (3)$$

$$\delta^2 = r_0^2 + 4\nu t \quad (4)$$

Where r_0 is the initial vortex radius (at $t=0$) and ν is the kinematic viscosity.

Figure 1 presents experimental data and a curve fit of the vertical velocity profile taken between the centers of the vortex pair as measured experimentally (and along the horizontal line, as shown in figure 3). The fitted curves for the wall-normal velocity, v, are in the form:

$$v = v_\theta = \frac{\Gamma_1}{2\pi(x-x_1)}\left[1-\exp\left(-\frac{(x-x_1)^2}{\delta_1^2}\right)\right] + \frac{-\Gamma_2}{2\pi(x+x_2)}\left[1-\exp\left(-\frac{(x+x_2)^2}{\delta_2^2}\right)\right] \quad (5)$$

Which resulted in $R^2=0.99$, where x_1 and x_2 are the vortex centers and δ_1 and δ_2 are the vortex radii. Note also that we do not limit our discussion to identical circulation vortices or even radii, since inclined and non-straight excitation slots will generate uneven vortices.

Figure 1 shows vorticity contours calculated from experimental PIV data (snapshot, phase locked, [2]) showing velocity vectors also. The jet emanating from the actuator slot and the vortex pair can be clearly identified. The dashed horizontal and vertical lines represent the lines on which velocity and vorticity data was extracted and fitted, in figures 2 and 3 respectively.

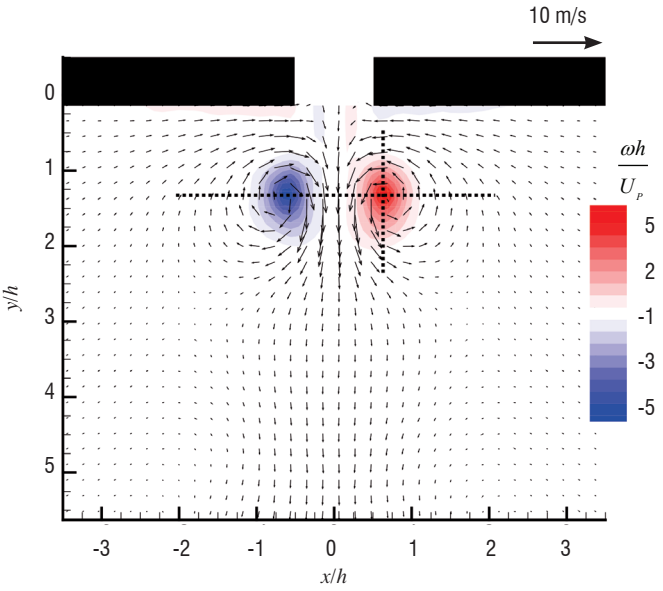

Figure 1 - Velocity vectors and vorticity contours of wall-normal excitation in still-air [2], The dashed lines represent the locations of the velocity profiles that were fitted and presented in figures 2 and 3. The slot width h=1mm.

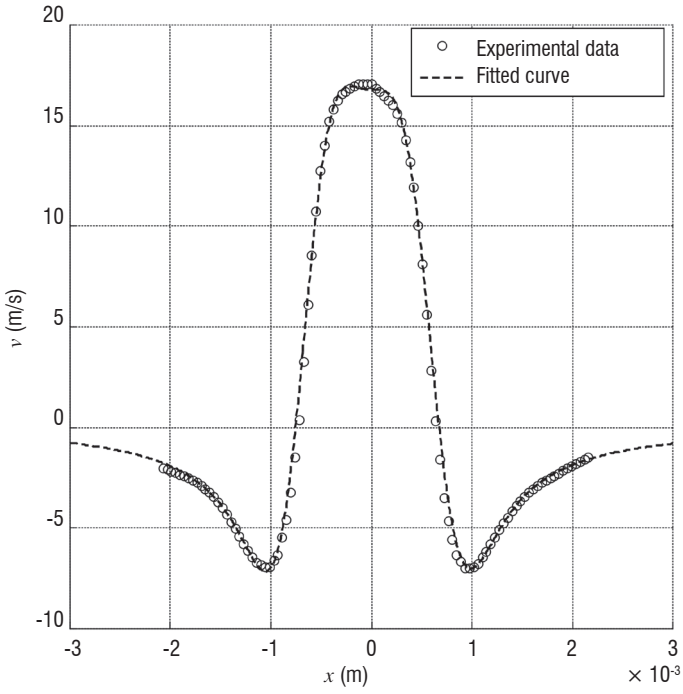

Figure 2 - Vertical velocity at t/T=0.625 (with respect to the velocity cycle at the slot) and its Lamb-Oseen curve fit (Eq. 5). Wall-normal excitation, $St=fh/U_p$=0.059 (f=1060Hz), with $ReU_p=hU_p/\nu$ =1200 (U_p=18m/s) in still-air. Where h is the slot width h=1mm), f is the excitation frequency, Up is the slot peak velocity and ν is the kinematic velocity

In order to validate the model, a Gaussian distribution was fitted to the vorticity profile calculated from the PIV measured velocities, along the horizontal line that is shown in figure 1. The vorticity profile and the

fitted curves are in very good agreement, as can be seen in figure 3. It is stressed that while the Lamb-Oseen vortex model is strictly valid in axis-symmetric flow and therefore at large distances between the vortex centers, we will use it empirically to model the current vortices, even when the distance between the vortices forming the pair is of the same order as their diameter. The results shown in figures. 1-3 clearly show the suitability of the Lamb-Oseen vortex model to describe the evolution of a single vortex forming a vortex-pair in still air. In the following sections, each vortex is modeled independently and symmetry is not imposed. It should be mentioned that the fit between the experimental data and the empirical Lamb-Oseen model are not always as good as seen in figures 2-3 and a comprehensive uncertainty analysis has not been performed. Furthermore, in the subsequent model the circulation, Γ_0, is not constant as in the original Lamb-Oseen model, but rather it is allowed to be *empirically* time dependent, according to the experimental findings in still-air.

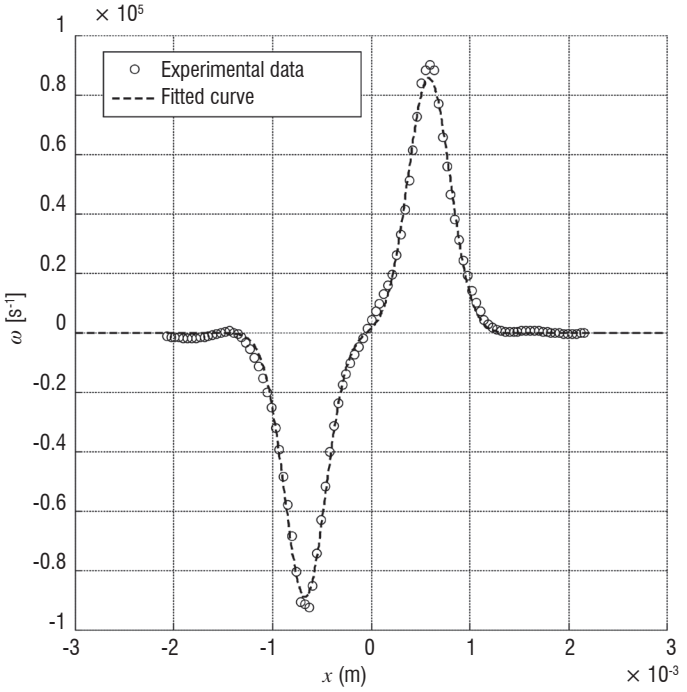

Figure 3 - Vorticity distribution at t/T=0.625 (with respect to the velocity cycle at the slot) and its Lamb-Oseen curve fit (eq. 2). Wall-normal excitation, St=0.059 (f=1060Hz), with Re_{U_p}=1200 (U_p=18 m/s) in still-air.

Four vortex interaction model

We initiate the analysis once the vortices have formed near the slot exit and define a system of four Lamb-Oseen vortices, as shown in figure 4. Each vortex in the system is defined according to eqs. 1-5. The wall is modeled as a symmetry line along the x axis, at y=0. The existence of the excitation slot is not included in the current state of the model.

The empirical justification to use the above approach stems from the success of the two vortex model to simulate still-air experiments. Hence, we attempt to expand it, although we do not use point vortices. Obviously, in viscous fluid, four vortices with no wall are not equivalent to two vortices and a wall. The assumption should be that the distance of the vortices from the wall is large compared to their diameters. Since this is not the case presently, we still have to convince the reader that the model works out of its designed range of formal applicability.

Let us consider the kinematic equations of motion for the 1st vortex, with a circulation $\Gamma_{0,1}\equiv\Gamma_0$, as described by its position vector $\vec{x}_1=(x_1,y_1)$. Once the position vector for the 1st vortex is defined, as well as its circulation, the following statements can be made regarding the four-vortex model, as shown in figure 5:

1. The coordinates of the other vortex forming the pair are given by $\vec{x}_2\equiv(x_2,y_2)=(-x_1,y_1)$, and its circulation is given by $\Gamma_{0,2}=-\Gamma_{0,1}$;
2. The images of vortices 1 and 2 are represented by vortices 4 and 3, respectively. Their coordinates are given by $\vec{x}_3\equiv(x_3,y_3)=(x_2,-y_2)$ and $\vec{x}_4\equiv(x_4,y_4)=(x_1,-y_1)$, and their circulations are given by $\Gamma_{0,3}=-\Gamma_{0,2}$ and $\Gamma_{0,4}=-\Gamma_{0,1}$.

Once all the vortex positions and circulations are defined, the kinematic equations of motion for Vortex 1, due to the induced velocities from the other three vortices in the system, can be written in the following manner, in terms of x_1, y_1 and Γ_0 only:

$$\dot{y}_1=\frac{\Gamma_0}{2\pi}\left\{\frac{1}{2x_1}\left[1-\exp\left(-\frac{4x_1^2}{r_0^2+4\nu t}\right)\right]-\frac{x_1}{2\left(x_1^2+y_1^2\right)}\left[1-\exp\left(-\frac{4\left(x_1^2+y_1^2\right)}{r_0^2+4\nu t}\right)\right]\right\} \tag{6a}$$

$$\dot{x}_1=\frac{\Gamma_0}{2\pi}\left\{-\frac{1}{2y_1}\left[1-\exp\left(-\frac{4y_1^2}{r_0^2+4\nu t}\right)\right]+\frac{y_1}{2\left(x_1^2+y_1^2\right)}\left[1-\exp\left(-\frac{4\left(x_1^2+y_1^2\right)}{r_0^2+4\nu t}\right)\right]\right\} \tag{6b}$$

In a similar manner, the motion of all other vortices can be calculated using the above definitions, as presented hereafter.

The peak vorticity magnitude of a single vortex model is found by substituting r=0 into eq. 2:

$$\omega_{\max}=\frac{\Gamma_0}{\pi\left(r_0^2+4\upsilon t\right)} \tag{7}$$

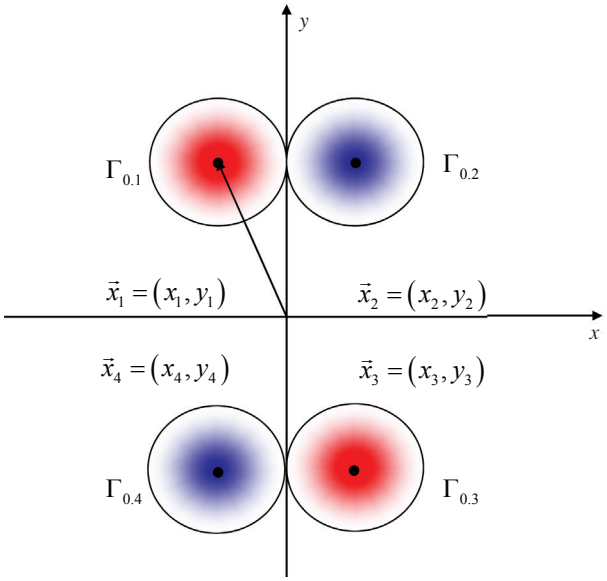

Figure 4 - A system of four Lamb-Oseen vortices

One of the prime targets of the current effort is to empirically model the time development of the experimental interaction of a vortex-pair with a cross-flow laminar boundary layer, including the time evolution of the vorticity. The initial vortex position vector is $\vec{x}_i(t=0)$.

The equations of motion for the vortices, as described above, can be written as a combination of the induced velocities at the vortex position. It is possible to calculate the motion of the *i-th* vortex in the above system using the following general equations:

$$\dot{\vec{x}}_i = \sum_{i \neq j} \vec{u}_j^{ind}\left(\left\|\vec{x}_i - \vec{x}_j\right\|, \Gamma_{0,j}(t)\right) \quad (8a)$$

$$\dot{\Gamma}_{0,i} = \dot{\Gamma}_{0,i}^{Baseline} \quad (8b)$$

The induced velocities are calculated from a vector summation of eq. 1 (or according to eqs. 6a and 6b). Equation 8 simply states that the motion of the *i-th* vortex is due to the superimposition of the induced velocities by the other three vortices (meaning the counter rotating vortex-pair and their corresponding images) and the velocity of the boundary layer at the vortex core locations (when the boundary layer free-stream velocity $U_e \neq 0$). Within the framework of the current model, a time dependent circulation of the *i-th* vortex, $\Gamma_{0,i}(t)$ is used. The evolution of the vortex circulation is obtained from the still-air experiments and used as input to the empirical four-vortex boundary layer interaction model. This is due to the Lamb-Oseen vortex model, which does not allow the circulation to decay during its entire "lifespan", whereas the measurements [2-4] clearly show that the vortex circulation decays with time. Modeling the physical mechanism that is responsible for the circulation decay is beyond the scope of this paper.

The time dependent vortex radius, $\delta(t)$, which is affected only by diffusion in the original Lamb-Oseen model, should grow with time to account for vorticity diffusion, but not dissipation.

From the experimental observations, one can hypothesize that the vortex evolution and resulting circulation is affected by several factors. The vortices do not remain circular, but rather they become elliptic, especially when they are very close together. To better represent experiments, the model vortices remain circular, but when compared to the experimental data, their circulation is reduced artificially using the "proximity factor", which will be discussed in the following section.
In the following section, we define and examine the meaning of each parameter affecting the vortex boundary layer interaction.

Vortex Circulation

The calculation of the vortex circulation was performed numerically on experimental findings. The termination of the surface integral of the vorticity distribution should be performed at a comparable level of vorticity, as compared to the peak vorticity of the vortex at that specific time and location, $\omega_l/\omega_{max}(t)$. A relative level $\sim O(10^{-2})$, was used throughout. Sometimes, a line rather than surface integral was used, according to the Stokes theorem:

$$\Gamma = \int_{A_{vortex}} \omega(x,y)\,dA = \oint_c \vec{u}.\vec{dl} \quad (9)$$

One can define the parameter A_{vortex} as the area enclosed by a contour C that corresponds to 1% $\omega_{max}(t)$ vorticity. In the model, this curve is always circular, as required by the undisturbed Lamb-Oseen vortex model.

In order to allow comparison of the model results to experiments, several ad-hoc assumptions need to be made. While in the model, the vortices are assumed circular;, they are not measured as such in the experiments. When the vortices are close together, they appear elliptic. In order to allow a comparison between the linear model (in which the circulation cannot alter due to the Helmholtz condition), a "proximity factor" was introduced. The mechanism, to be detailed below, is not used to alter the vortex circulation in the model, but rather only to compare the model results to the experiments once the model results have been obtained. Furthermore, the trajectories of the model are compared to the experiments without any assumption or correction.

Figure 5 presents two cases: (a) a single Lamb vortex and (b) two similar "near-by" counter-rotating Lamb vortices (with the same peak vorticity magnitude as in case (a), but of opposite sign). The same minimum vorticity level, ω_l, is presented in figures. 5a and 5b for each case (as the red line).

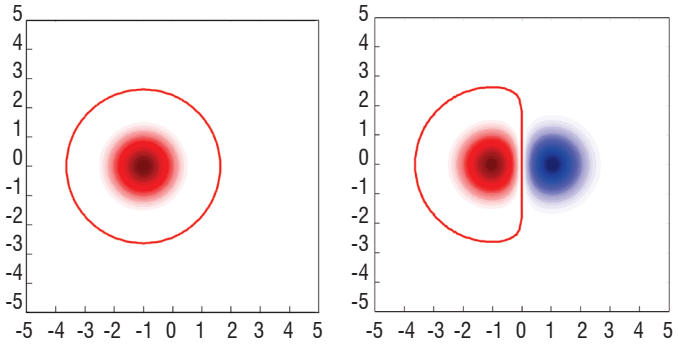

(a) A single Lamb vortex (b) Two near-by counter-rotating Lamb vortices

Figure 5 - A sketch showing the partial mutual cancellation of two nearby counter-rotating "Lamb" vortices with similar initial circulation (Γ_0, according to eq. 5) was used in both cases. The solid line represents the vorticity level ω_l

Clearly, the calculated circulation of the positive ("red") vortex will not be the same in both cases, due to the overlap of the vorticity from the opposite signed vortex, even though Γ_0 is identical in both cases. A sequence of such cases was analyzed, in order to calculate the effect of the proximity factor, s/δ (where s is the distance between the vortex centers, and δ is the undisturbed vortex radius), on the resulting calculated circulation, as measured in the experiments and calculated from experimental data. Figure 6 presents the ratio between the calculated circulation and the proximity factor.

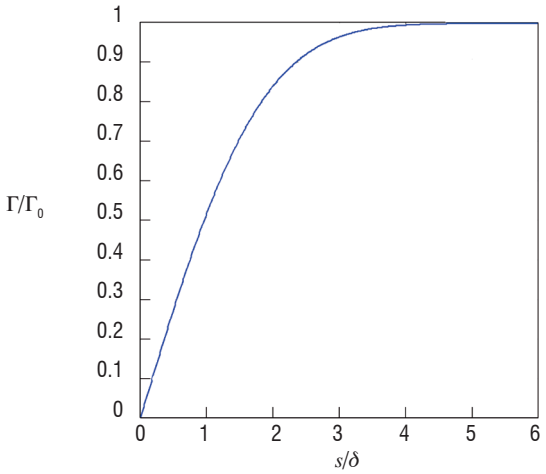

Figure 6 - Circulation reduction "measurement" due to the proximity (s/δ) between two counter rotating "Lamb-Oseen" vortices. δ is the calculated circulation; Γ_0 is the model circulation, as substituted into eqs. (1)-(3)

Naturally, when the distance between the two vortices is zero, the vortices completely overlap in such a way that the circulation calculated on a surface containing both becomes null. Generally, this is the case in any other closed line containing two identical magnitudes and opposite signed 2D vortices. Also, when the distance is large enough, say $s/\delta>5$, the vortices do not overlap. When the distance between the vortex centers is O(1), as seen experimentally, some 50% of the circulation, measured around one of the vortices only, should be reduced in order to match the experiments.

A vortex-pair in still-air

In order to fit the parameters of the Lamb-Oseen vortex model to the experimental data, the time evolution of the vortex circulation, $\Gamma_0(t)$, and the initial vortex radius, r_0, should be extracted from the phase-locked PIV data. These parameters, with the effect of the "proximity factor" (increasing the circulation to be used in the model with respect to the experiment) should enable the prediction of the flow field evolution reasonably well, initially in still-air.

The time evolution of the vortex-pair circulation in still-air for the wall-normal excitation, is presented in figure 7a. Previous publications have shown that the circulation time evolution is fairly self-similar (for the cases where the excitation magnitude is supercritical, i.e., the vortices "escape" the suction effect) for several boundary conditions. In a modeling effort, the critical vortex formation condition can be predicted for both line and ring vortices, using the St-Re condition of Holman et al. [5]. In contradiction to known vortex models, the circulation of the vortices forming the vortex-pair, even in still-air, decays with time in experiments. This decay could be explained by several possible mechanisms. First, partial overlap of the vorticity with opposite signs forming the pair, once the distance between the vortices forming the pair is smaller than two diameters. It was established however, that this effect cannot explain the magnitude of the circulation decay. Interaction with residual circulation of opposite sign at the vicinity of the slot and the effect of viscosity induced decay can also affect it. Three-dimensional effects, transition to turbulence and interaction with turbulent structures can also reduce the measured circulation. Certainly, under turbulent flow conditions, the 2D assumption no longer holds.

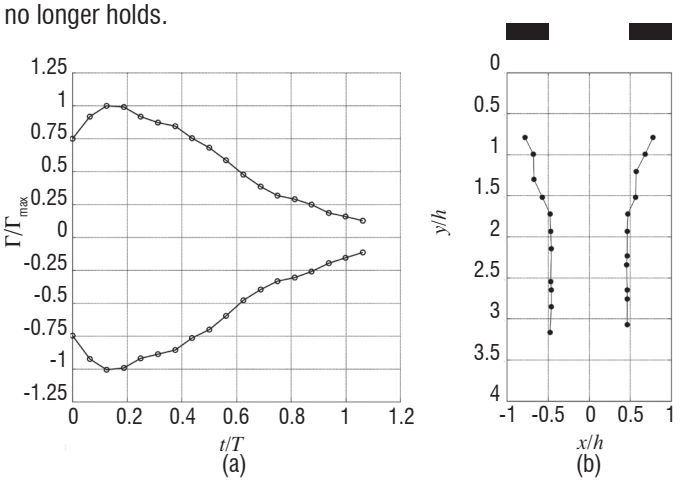

Figure 7 - (a) Normalized computed circulation time evolution for the PIV measured wall-normal excitation and (b) vortex trajectories (the left curve is that of the negative circulation vortex and the right one is for the positive one). U_p=18[m/s] f=1060[Hz]. The slot is 1h wide (h=1mm) and centered on (0,0)

In this paper. t=0 is defined as the first instant when a coherent vortex can be detected in the flow field (and not when V=0 at the center of the slot exit and at the beginning of the blowing cycle). The time lag between the initiation of the blowing velocity cycle at the slot and the formation of a vortex at the vicinity of the slot must be modeled using detailed experiments, CFD and available theoretical considerations. Experimental vortex trajectories are presented in figure 7b, where the vortex location was identified by the peak vorticity (and not by the peak angular momentum, as presented in previous publications by the current authors, due to modeling convenience).

The time evolution of the circulation computed from the experimental data in still-air, using a surface integral on the vorticity, as presented in figure 7a, might be biased due to the effect of partial overlap of the vortex vorticity, as discussed above. Therefore, a "proximity factor" s/δ (where s is the distance between the two vortex centers and δ is the vortex radius) is introduced and it could be computed from the trajectories presented in figure 7b. An initial estimation of this distance, based solely on the initial vortex locations, can be computed from the Lamb-four-vortex model [10] or by the Karweit [11] and Sheffield [12] models.

An additional variable that must be defined for the subsequent computation of the proximity factor is the vortex radius, $\delta(t)$. The Lamb-Oseen model states that the vortex radius increases due to diffusion, according to $\delta^2(t)=r_0^2+4\nu t$. Lamb-Oseen vortex models had been fitted to the measured vorticity field in two directions. Clearly, it is desired to calculate a representative radius based on some integral feature, but the procedure below is used merely in order to establish the limits. The first fit was on a horizontal dashed line passing through the centers of the two vortices, as shown in figure 1, and according to eq. 5a, as shown in figure 3.

The second type of fit was performed along the vertical line passing through the center of the positive vortex, as shown by the vertical dashed line in figure 1, and was in the form:

$$\omega(y)=\frac{\Gamma_1}{\pi\delta_1^2}\exp\left(-\frac{(y-y_1)^2}{\delta_1^2}\right) \qquad (10)$$

The resulting estimations for the vortex radius obtained from the above-mentioned fits are presented in figure 8b. One can note that there is a significant difference in the results according to the two methods for estimating $\delta(t)$. One should recall that the Lamb-Oseen vortex model is axisymmetric. The experimentally measured vortices undergo a significant stretching in the wall-normal direction as they travel away from the slot and therefore the radius in the wall normal direction increases significantly, as shown in figure 8b, while the radius in the horizontal direction remains approximately constant (these two directions could also be considered to be related to the small and large axes of an ellipse), as is also shown in figure 8b. The resulting circulation, calculated for a Lamb vortex with diameter obtained from a vertical (y) profile, will be significantly larger than that calculated according to a vortex radius calculated using the radius obtained from a cut through the vortex in a horizontal plane. The same magnitude of the vorticity peak is used in the model, regardless of its stretching. An example of this effect is shown in figure 8a. Three sets of data are shown. The "numerical integration" is calculated directly from the experimental data. The two other sets are calculated assuming a circular Lamb vortex, with the same peak vorticity but with $\delta(t)$ from figure 8b. The differences are self-explanatory. Currently, the vertical cross-section through the vortex core (along the dashed vertical line in figure 1) is used to evaluate the vortex radius. The linear fit to the vortex radius, as computed by the horizontal cut through the experimental vorticity data, is:

$$\delta^2 = 5.1*t/1000+8.7*10^{-8} \quad (11)$$

Its slope is significantly larger than 4ν (the radius squared, according to eq. 4, is also shown in figure 8b), but the evolution is linear, as Lamb's model requires. The above equation represents a much faster expansion rate than the Lamb-Oseen vortex model predicts, because it accounts only for laminar vorticity diffusion. As a first order approximation, the model for the vortex radius, as expressed in eq.11, is used for the following computations to be subsequently presented. We will allow the slope of to vary, in order to better fit the data of the vortex-boundary layer interaction. Other vortex pair data sets are required to formulate a more general form of the vortex radius. The logic for allowing the same trend but with a different viscosity could be justified on similar arguments that lead to the widely accepted turbulent eddy viscosity model. Higher turbulence levels could also explain the rapid decay rate of the circulation. Figures 9a and 9b present the resulting proximity factor, s/δ, and the ratio between the model circulation and the expectation to the measured circulation, Γ_{exp}/Γ_0, as a function of time, respectively. One can note that the experimentally measured vortices are expected to show approximately 30% lower circulation in comparison to their potential counterpart, due to the partial overlap (figure 9b).

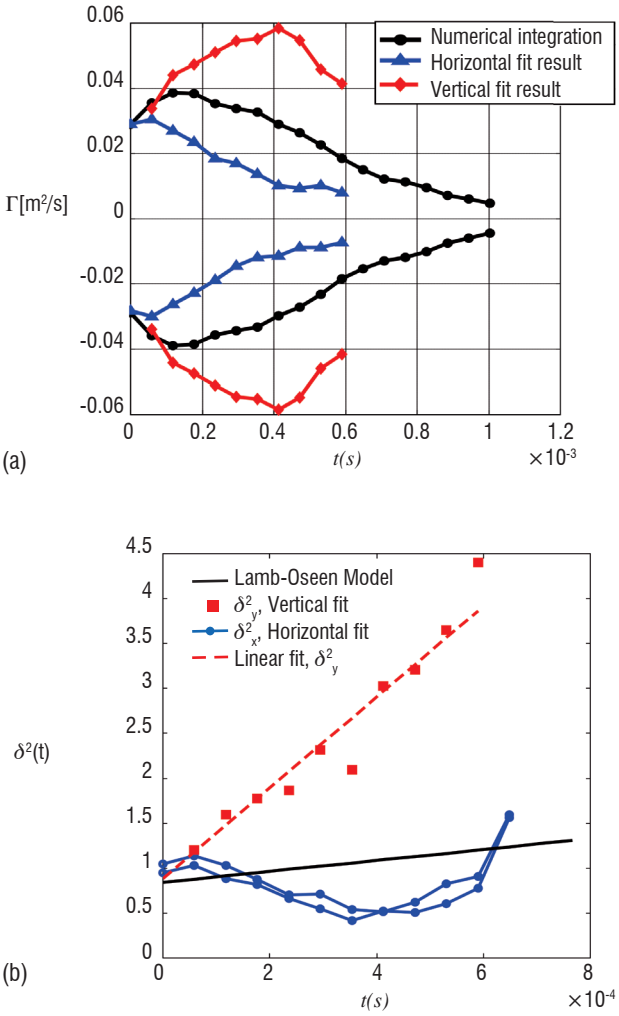

Figure 8 - (a) Circulation time evolution comparison for wall-normal excitation, as fitted by horizontal and vertical profiles and as computed using 2D integration scheme. (b) Radii of the vortices, as fitted by horizontal and vertical profiles. The black line in (b) is $\delta^2(t) = r_0^2 + 4\nu t$, with r_0^{-1}

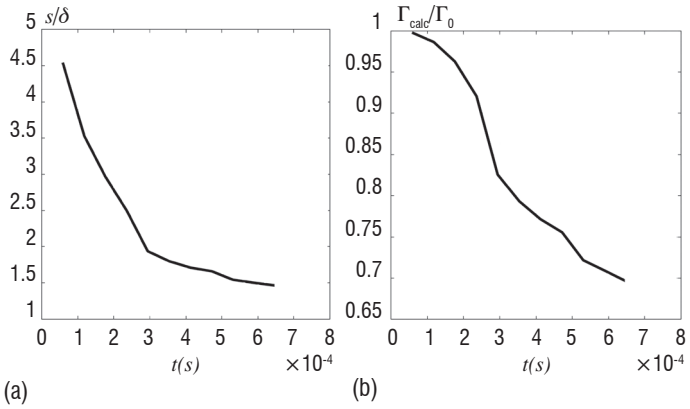

Figure 9 - (a) The experimental proximity factor for the vortex-pair in still-air using the factor shown in figure 6 on the data of figures 7b and 8b (for the distance between the cores and the vortex radii), respectively and (b) the "experiment" circulation calculated using the proximity factor in (a) applied to the experimental model

The time evolution of the "corrected" circulation, to be computed from the model assuming a circular rather than squeezed elliptic vortex, is presented in figure 9c. The model peak circulation must be increased by about 15% compared to the experimentally computed circulation and it also occurs at a later time. Furthermore, the circulation used in the model is essentially constant for about half of an excitation cycle (~0.5 msec) and is significantly attenuated at later times.

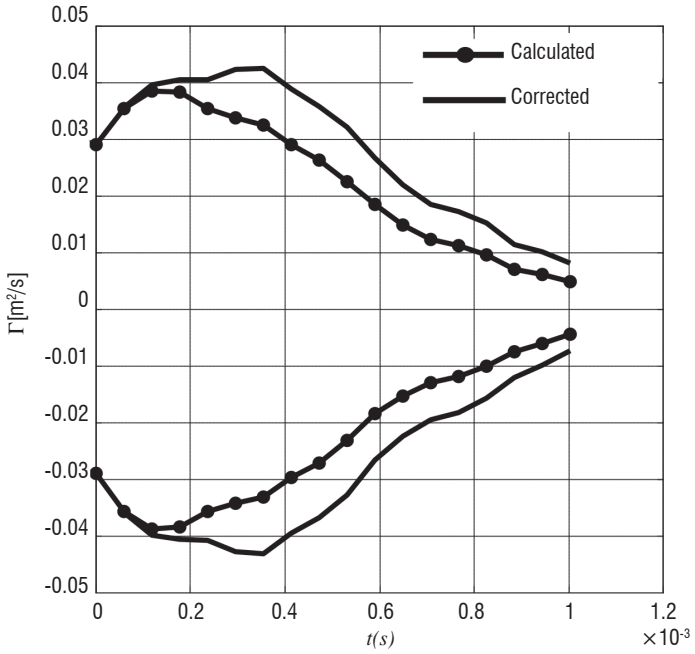

Figure 9c - Comparison between the experimentally calculated and corrected model circulation curve

The "corrected" circulation from the still-air experiments (figure 9c), as well as the expression for the vortex radius (eq.11), were introduced into the four-vortex model as described above, in order to validate and calibrate the model that will be used for the excitation interaction with the cross-flow, initially against the still-air data .

A Gaussian curve was fitted to the "corrected" circulation curve (as shown in figure 9c) for the convenience of subsequent numerical treatment.

Figures 10a and 10b present the trajectories and time evolution of the circulation, as predicted by the current four-vortex model and compared to the still-air findings.

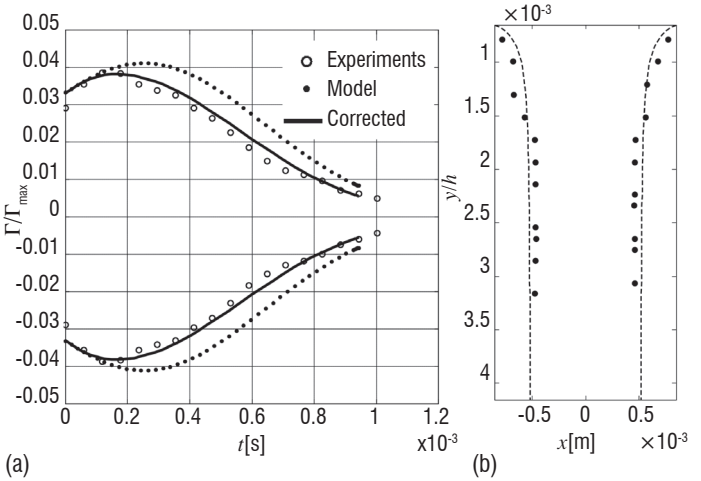

Figure 10 - (a) Model vs. Experimental circulation time evolution. "Model" here is the fitted Gaussian. "Corrected" is the circulation values with the partial overlap factor included. (b) Vortex trajectories from the model compared to experiment

It should be noted that the model circulation represented by the dots in figure 10a is larger than the experimentally computed circulation. This correction takes into account the reduction in the measured vortex circulation due to their proximity. However, for the model adherence to the theoretical considerations and its linear implementation, the circulation that is used for the simulation is increased according to the proximity factor, shown in figure 9b. Using this vorticity time evolution, the model computes the convection velocities, flow fields, circulation (due to the superimposition with the boundary-layer) and more. However, if we intend to compare its circulation to the still-air PIV measurements, we must take into account the proximity that causes the 2D integration method to "measure" a smaller circulation due to the overlap region of the finite radius vortices. Once we account for the proximity factor and its effect on the circulation, we obtain the "corrected" model circulation, which is in very good agreement with the measured PIV data, as shown in figure 10a. The vortex trajectories, shown in figure 10b, are in very good agreement with the experiments. Finally, the data shown in figures 10 merely serves as indication of the model fidelity and the reliability of its numerical implementation.

Interaction of a vortex-pair with cross-flow

The approach for modeling the vortex-pair in the proximity of the wall and interacting with a cross-flow boundary layer is outlined below. The expansion of the above four-vortex model is theoretically sound only if the cross-flow (boundary-layer) velocity is assumed to be constant. However, currently it represents a realistic shear flow, the Blasius boundary layer. Hence, even if one considers potential models, many point-vortex interactions must be considered. Furthermore, the Lamb-Oseen vortex model is not a point-vortex model. To simplify this complex situation, we note that the Blasius boundary layer *vorticity*, under the current experimental conditions, is negligibly small as compared to the peak vorticity within the vortex cores (on the order of 30:1) and, hence, in the leading order approximation it is reasonable to neglect it. However, this residual boundary layer vorticity will alter the relative circulation of the vortices forming the pair, making one stronger than the other, and the pair will eventually rotate.

The interaction of the vortices with the boundary layer is modeled by the following procedure;

1. Define the initial vortex positions, $\vec{x}_i(t=0)$ (where i=1,2 represent the counter rotating vortices and i=4,3 represent their images, meaning $\vec{x}_3=(x_2,-y_2)$ and $\vec{x}_4=(x_1,-y_1)$.
2. Define the initial vortex circulations, $\Gamma_{0,i}(t=0)$ (where i=1,2 represent the counter rotating vortices and i=3,4 represent their images, meaning $\Gamma_{0,3}=-\Gamma_{0,2}$ and $\Gamma_{0,4}=-\Gamma_{0,1}$) at any time.
3. Define the initial vortex radius, r_0 (currently identical for all vortices).
4. Calculate the time derivatives of the vortex locations and circulations in accordance with the following equations:

$$\dot{\vec{x}}_i=\sum_{i\neq j}\vec{u}_j^{ind}\left(\left\|\vec{x}_i-\vec{x}_j\right\|,\Gamma_{0,j}\right)+\vec{U}_{BL}\left(\vec{x}_i\right) \quad (12a)$$

$$\dot{\Gamma}_{0,i}=\dot{\Gamma}_{0,i}^{Baseline}+\oint_{C(t)}\omega_{BL}\left(\vec{U}_{BL}-\dot{\vec{x}}_i\right)\cdot d\vec{l} \quad (12b)$$

where the vortex radius can be calculated in each time step according to eq. 11.

5. Use a time marching numerical scheme to integrate equations 12a and 12b.

Note that the expression $\oint_{C(t)}\omega_{BL}\left(\vec{U}_{BL}-\dot{\vec{x}}_i\right)\cdot d\vec{l}$ in eq. 12b is the vorticity flux along the vortex boundaries $C(t)$. When there is no boundary layer, $\vec{U}_{BL}=0$, it is required that $\omega_{BL}(x,y)=0$ also, and eq. 12 reduces to the form of the still-air four-vortex model, as presented in eq. 8.

The above procedure allows the vortex circulation to effectively vary according to the level of the background boundary layer vorticity, according to the vorticity transport equation.

The following figures (11-12) show the vortex trajectories and circulation due to the interaction of the vortex-pair with a cross-flow Blasius boundary layer. The integral parameters of the boundary layer at the entrance to the computed domain were matched to the experimental baseline (undisturbed) boundary layer. The vortex pair evolution was computed according to steps 1-5, as defined above.

The initial conditions used for both simulations are provided in Table 1 below. Note that we have allowed an initial circulation difference between the vortices, in order to better account for the effect that the boundary layer vorticity has on the vortex circulation during the formation period, as seen experimentally.

As in the Lamb [10] model and the results of the still-air simulation, the vortices initially become closer due to the image vortices as they are carried away from the wall, due to the mutual induction. The effects of the cross-flow are twofold. The trivial effect is the downstream convection, which is height (y) dependent. The other effect is the alternation of the vortex circulation to account for the effect of the baseline boundary layer vorticity, as defined in step 5 above and seen in figure 11a. The overall agreement between the model and the experiment is fair, especially the evolution of the negative vortex, which is crucial to explain effects on a separating boundary layer.

Variable	Description	Case 1 (fig.11)	Case 2 (fig.12)
Ue	Free-stream velocity [m/s]	5.5	8.3
x_1	Initial x location, Positive vortex [mm]	0.9	0.9
y_1	Initial y location, Positive vortex [mm]	0.67	0.63
x_2	Initial x location, Negative vortex [mm]	0.95	0.86
y_2	Initial y location, Negative vortex [mm]	0.55	0.54
$\Gamma_{0.1}$	Initial circulation, Positive vortex [mm]	0.027	0.03
$\Gamma_{0.2}$	Initial circulation, Negative vortex [mm]	-0.032	-0.035

Table 1: Initial conditions for the two cases of excitation-vortex-pair interaction

It could be noted that initially, the agreement between the trajectory of the negative vortex and the experimental trajectory is not as good, possibly because the blockage effect that the positive vortex has on the boundary layer is not taken into account in the linear model. Additional effects that are not taken into account are the possible alternation of stationary vortex circulation, due to net vorticity transport across its boundaries and dissipation at the wall.

The circulation that is used for the model is marked by the dashed red and blue lines, in both figures 11 and 12, while for the sake of comparison to the experiment, it is multiplied by the proximity factor, calculated for the trajectories in the presence of cross-flow.

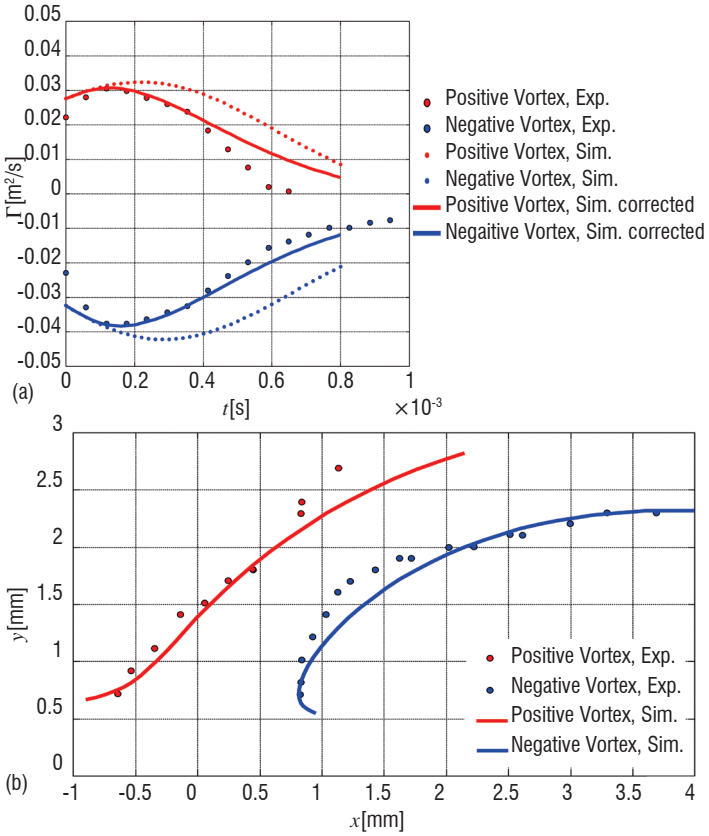

Figure 11 - The evolution of the vortex pair circulation (a) and trajectories (b) for vortex-boundary layer interaction, Case 1. U_p=18 m/s and U_e=5.5 m/s

Figures 12a and 12b present the vortex-pair boundary-layer interaction, with the same excitation parameters that were used in still-air and in the Case 1 cross-flow experiment, only for Ue=8.3m/s as the free-stream velocity. The remaining parameters are provided in Table 1. Due to the larger free-stream velocity, the trajectories are bent more towards the wall and into the downstream direction. The circulation of the two vortices diverges faster than in the lower free-stream velocity, due to the increased vorticity of the background boundary layer.

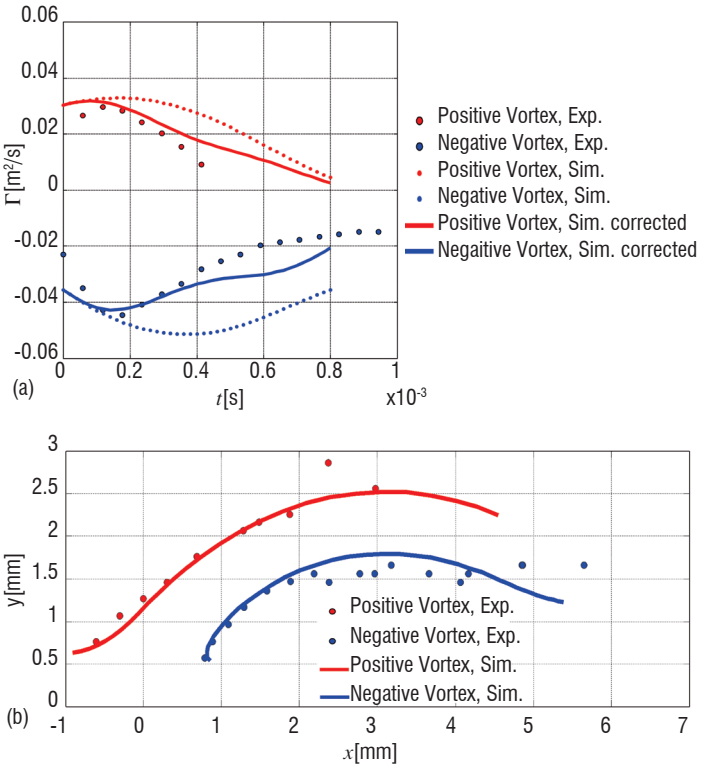

Figure 12 - The evolution of the vortex pair circulation (a) and trajectories (b),for vortex-boundary layer interaction. Case 2. U_p=18m/s and U_e=8.3m/s.

The interaction dynamics can be interpreted as follows. The vortex-pair starts to be convected in the wall-normal direction, due to the mutual induced velocities. The image vortices induce velocity mainly in the x direction, bringing the vortices closer. The boundary layer velocity in the initial position (and at the initial time) is small, compared to the induced velocities by the vortex-pair. As the Vortices move away from the wall, their circulation changes, due to the interaction with the boundary layer vorticity. The positive vortex decays because a negative vorticity flux "enters" its boundaries, whereas the negative vortex intensifies due to the same reason. This difference in the circulation causes the vortices to move along a curved trajectory (actually a circular trajectory whose radius increases with the difference of their circulation) as shown in figures 11b and 12b. The experiments show that the positive vortex circulation decays very fast (0.4-0.5[ms], figures 11a, 12a), within less than one excitation cycle. Therefore, the positive vortex ceases to induce velocity on the negative vortex and the negative vortex travels downstream with the boundary layer, almost parallel to the wall. However, the model does not seem to be capable of predicting the rapid decay seen experimentally. It is highly probable that after t>0.5 ms, 3D effects start to be important and other mechanisms cause the positive vortex to lose its circulation so rapidly.

The vortex dynamics highly depend on the initial conditions. If one starts the simulation closer to the wall, the wall images play a stronger role on the vortex convection velocities, making them reside longer in the presence of the stronger boundary layer vorticity and therefore exposing their circulation to the boundary layer vorticity for a longer

time. This will cause the positive vortex circulation to decay faster, until it vanishes in the boundary layer, and will cause the negative vortex circulation to rapidly grow.

Conclusions

A model for describing the evolution of a vortex-pair during the interaction with a laminar boundary layer was proposed, calibrated and validated against experimental data. The model is similar to the Lamb four-vortex model, adopted for finite radius vortices. One exception is that the vortex circulation is empirically allowed to vary with time, according to the experimental findings. This model explains the initial motion of the vortices towards each other in the proximity of the wall. The inclusion of the boundary layer effects is performed through two mechanisms. The first is vortex convection and the other is superimposition with the background boundary layer vorticity. The latter is altered as the vortex travels across the boundary layer. This approach can be implemented because the boundary layer vorticity is negligibly small compared to the vortex magnitude. The initial circulation and its time evolution from the still-air model are used for the cross-flow interaction. In order to make a comparison between the model results, assuming circular vortices, and the experimental findings, in which the vortices are not circular, especially when close together, a correction factor was introduced. The model was compared to experiments for wall-normal excitation with reasonable agreement.

It was noted that the evolution of the vortices is very sensitive to the initial formation locations. The link between the characteristics of the slot excitation and the initial circulation and locations of the vortices should be modeled, in order to allow the development of the current model with a simplified boundary condition for CFD simulations and further development as a low-order-model for flow control purposes■

Acknowledgements

The authors would like to thank G. Zilman and G. Iosilevskii for many helpful discussions and suggestions.

References

[1] P.G. SAFFMAN - *Dynamics of Vorticity.* 1981, JFM 106; pp. 49-58.
[2] T. YEHOSHUA, A. SEIFERT - *Boundary Condition Effects on Oscillatory Momentum Generator.* AIAA Paper 2003-3710, June 2003.
[3] T. YEHOSHUA, A. SEIFERT - *Active Boundary Layer Tripping Using Oscillatory Vorticity Generator.* Aerospace Science and Technology, 10 (3): 175-180 APR 2006a.
[4] T. YEHOSHUA, A. SEIFERT - *Boundary Condition Effects on the Evolution of a Train of Vortex Pairs in Still Air.* Aeronautical J., 110 (1109): 397-417 JUL 2006b.
[5] R. HOLMAN, Y.UTTURKAR, M.R. MITTAL, B.L. SMITH, L. CATTAFESTA - *Formation Criterion for Synthetic Jets.* AIAA Journal, 2005, vol.43 no.10 (2110-2116).
[6] A. GLEZER - *The formation of vortex rings, Physics of Fluids*. December 1988 -- Volume 31, Issue 12, pp. 3532-3542.
[7] N.DIDDEN - *1979, On the Formation of Vortex Rings: Rolling-up and Production of Circulation.* ZAMP (Zeitschrift für Angewandte Mathematik und Physik), Volume 30, Number 1 / January, 1979.
[8] O.K. REDINIOTIS, J. KO, X. YUE, A.J. KURDILA - *Synthetic jets, their reduced order modeling and applications to flow control.* AIAA paper 1999-1000 , Jan., 1999 (also AIAA J. 2002).
[9] P. HOLMES, J.L. LUMLEY, G. BERKOOZ - *(1996) Turbulence, Coherent Structures, Dynamical Systems and Symmetry.* Cambridge University Press, Cambridge, Great Britain,1996.
[10] H. LAMB - *1932 Hydrodynamics*. Dover.
[11] M. KARWIET - *Motion of a vortex pair approaching an opening of a boundary*. Phys. Fluids, 18: 1604-6, 1975.
[12] J.S. SHEFFIELD - *Trajectories of an Ideal Vortcx Pair Near an Orifice*. Phys. Fluids 20 : 543-545, 1977.
[13] E.J. ROUTH - Proc. Lond. Math. Soc. 12, 73, (1881).
[14] P.G. SAFFMAN - *Vortex Dynamics.* Cambridge University Press, 1992.
[15] K. SHARIFF, A. LEONARD - *Vortex Rings*. Ann. Rev. Fluid. Mech., Vol. 24: 235-279, 1992.
[16] G.K. BATCHELOR - *An Introduction to Fluid Dynamics*. Cambridge University Press (§4.5) 1967.
[17] R. KARAGOZIAN, ANN - *Progress in Energy and Combustion Science*. 36 ,531-553 (2010).

Nomenclature

x,y	Coordinates along a 2D axis
x_i, y_i	Vortices locations
v_θ	Circumferential velocity component
ω	Out-of-plane vorticity component
Γ	Circulation
Γ_0	Initial Circulation
δ	Vortex radius
r	Radial coordinate
r_0	Vortex radius at t=0
t	time
h	Actuator's slot width
U_p	Peak Velocity at the actuator's slot
f	excitation frequency
ν	kinematic velocity
St	Strouhal number, fh/U_p
Re_{U_p}	Reynolds number based on U_p, hU_p/ν
T	Time of excitation cycle, $1/f$
$\dot{(\,)}$	Time derivative
$\vec{u}^{IND}$	Induced velocity
$\Gamma_0^{Baseline}$	Vortex circulation as a function of time for a baseline flow, Ue=0.
U_e	Boundary layer free-stream velocity
A_{vortex}	Area enclosed by a contour C that corresponds to 1% $\omega_{max}(t)$ vorticity
ω_l	Vorticity level
s	Distance between the vortices' centers
R^2	Correlation factor
ω_{BL}	Boundary layer vorticity
U_{BL}	Boundary layer velocity

AUTHORS

Avrahame Seifert is a Professor of Mechanical Engineering at Tel Aviv University and also the head of the Meadow Aerodynamics Laboratory. Prof. Seifert is an expert in low speed Aerodynamics and Active Flow Control. Dr. Seifert is developing methods and devices to alter the natural development of flows using localized, minute, unsteady energy expenditure, utilizing flow instability instead of brute force. Prof. Seifert received his entire education at Tel Aviv University, before leaving for a post-doc at NASA Langley. He has been a member of the Faculty at Tel Aviv University since 1999. Dr. Seifert has published close to 50 peer-reviewed Journal papers, has 5 patents (several more pending) and has educated more than two dozen graduate students. Prof. Seifert served as the Vice Dean for Research & Engineering and now serves as the Head at the School of Mechanical Engineering. His recent research interests focus on energy aspects of flow related systems and on the environment. Specifically, Aerodynamic drag reduction of heavy transportation systems (such as trucks, trains and buses) and enhanced effectiveness of wind turbines in urban settings and near transportation systems. Prof. Seifert is a world leader in developing actuators for flow control and four of his patents are in this area of R&D.
Personal homepage:
http://www.eng.tau.ac.il/~seifert/
Meadow Aerodynamics homepage:
http://www.eng.tau.ac.il/research/laboratories/Aerodynamics/

Tal Yehoshua is a Mechanical Engineering graduate student at Tel Aviv University. His main research interests are unsteady aerodynamics, flow control, boundary layers, vortical flows and flow instabilities, as well as optimization methods. Tal received his Bsc and Msc at Tel Aviv University and is currently leading several projects in the Aeronautical community in Israel.